

Diffraction limited 3D cell volume derivation for scattering data analysis

N.A.H.K. Rao^{*a}, M. Barbu-McInnis^{*a}, M. Helguera^{*a}, C.J. Daly^{*a}

^aChester F. Carlson Center for Imaging Science, Rochester Institute of Technology

ABSTRACT

Ultrasound speckle carries information about the interrogated scattering microstructure. The complex signal is represented as a superposition of signals due to all scatterers within a resolution cell volume, V_E . A crossbeam geometry with separate transmit and receive transducers is well suited for such studies.

The crossbeam volume, V_E is defined in terms of the overlapping diffraction beam patterns. Given the focused piston transducer's radius and focal distance, a Lommel diffraction formulation suitable for monochromatic excitation is used to calculate V_E as a function of frequency and angle. This formulation amounts to a Fresnel approximation to the diffraction problem and is not limited to the focal zone or the far field. Such diffraction corrections as V_E are needed to remove the system effects when trying to characterize material using moment analysis.

Theoretically, V_E is numerically integrated within the overlapping region of the product of the transmit-receive transfer functions. Experimentally, V_E was calculated from the field pattern of a medium-focused transducer excited by a monochromatic signal detected by a 0.5mm diameter PVDF membrane hydrophone. We present theoretical and experimental evaluations of V_E for the crossbeam geometry at frequencies within the transducers' bandwidth, and its application to tissue microstructure characterization.

Keywords: Cell volume, diffraction, Lommel functions, focused transducers, ultrasound

1. INTRODUCTION

In ultrasonic measurements a cell volume can be defined as the effective volume of a three dimensional region within which the interaction providing the echo data takes place. The radiation beam pattern of the transducer plays a major role in the definition of this cell volume. For example, in Fig. 1 two separate transducers are used to interrogate the scattering properties of a medium with a monochromatic signal. One operates as the transmitter and the other as the receiver. While the transmitter insonifies a region defined by its own radiation beam pattern the scattered signal is received by the receiver only from a limited portion of this region. This limited section gets defined by the geometrical positioning of the receptive beam pattern of the second transducer. In order to keep the calculations simple and tractable it is reasonable to assume point scatterers in the scattering medium. A given point scatterer will have a different amplitude response in this setup depending on where it is located within this overlap region. This difference should be attributed to the shape and form of the cell region and not to any possible statistical variations of the scattering strengths. This observation has two major implications. First, a scattering model based on a statistical derivation of the scattering cell volume has to be formulated. Secondly, it is important to realize that there will be an "effective cell volume" rather than a physical volume bounded within a closed surface. This effective volume is an averaging of sorts that takes into account the fact that the scatterer response varies at different spatial locations within the cell.

The objective of this paper is many fold. First, we present a model based derivation of an effective cell volume, see Eq. 9, in section 2. This is done for two circular disk focused transducers in a transmit-receive geometry subtending an angle. The significance of this cell volume in the moments analysis of the speckle data becomes clear from Eq. 8. Section 3 considers the Lommel diffraction formulation to calculate the transducer beam pattern terms necessary for the cell volume calculations. The significance of this formulation is presented

*narpci@cis.rit.edu; Phone 1 585 475-7183; fax 1 585 475-5988; Chester F. Carlson Center for Imaging Science, Rochester Institute of Technology, 54 Lomb Memorial Dr., Rochester, NY 14623.

in the discussion section 7. In section 4 we demonstrate how the two transducer parameters, namely effective diameter, a , and effective radius of curvature, A , can be derived from the hydrophone based diffraction field measurements¹. In section 5 we make a conceptual connection of the terms involved in the definition of the cell region with the imaging science definition of a point spread function (PSF)². This connection may be useful for those who would like to experimentally determine this cell region and is discussed in section 7. Section 6 presents some results on the theoretical calculation of this cell region as well as on the effective cell volume. The utility of the theoretical approach is demonstrated by performing calculations at different frequencies as well as at two different cross beam depths.

Some of the different aspects of our work can be related to work done by other researchers. We have done so in different sections wherever it is appropriate. The overall concept of a cell volume calculation has been attempted by Chen et al.³ for pulsed excitation in a back-scattering set up where $\theta = 0^\circ$. It is our hope that the concept of a cell volume will be very useful in many different diffraction as well as frequency and angle dependent scattering measurements.

2. SIGNAL FROM A RANDOM MEDIUM

The theoretical foundation for speckle statistics analysis under conditions of low scattering has been studied by Jakeman⁴, Chen⁵, and Waag⁶ among others. It is important to establish a relationship between the scatterer number density and other properties of the medium. Among these properties is the effective cell volume, which Chen and Campbell⁷ have defined in terms of narrow-band or short pulse excitations. In the work that follows, we institute a relationship between the normalized intensity moments and the effective scatterer number density using monochromatic excitations.

Prior to the analysis of the scattering signal, some essential assumptions are in order. First, assume that randomly distributed scatterers give rise to all echo signals, which means that the probability that a scatterer is at one position is the same as the probability that it is located at any other position. Second, multiple scattering is negligible and the waves scattered by each particle are spherically symmetric over the surface of the transducer. Further, the number of scatterers in the volume contributing to the scattered signal is assumed to be Poisson distributed. Finally, with the exception of small impedance discontinuities distributed randomly in space, the medium is assumed to be non-attenuating and uniform.

The scatter signal from the n^{th} scatterer is given by

$$s(t, r) = e^{2\pi j f_o t} \sum_{n=1}^M |H_T(\rho_n^T, \omega, z_n^T)| |H_R(\rho_n^R, \omega, z_n^R)| |\Psi_n(\omega)| |T_T(\omega)| |T_R(\omega)| e^{-2\pi j f_o \tau_n} \quad (1)$$

where $T_T(\omega)$ and $T_R(\omega)$ are the transmit and receive frequency response of the transducers. $\Psi_n(\omega)$ is the frequency dependent scattering coefficient of the n^{th} scatterer. $H_T(\rho_n^T, \omega, z_n^T)$ and $H_R(\rho_n^R, \omega, z_n^R)$ correspond to the diffraction terms presented in the following section under the Lommel diffraction formulation, where ρ_n^T and ρ_n^R are the off-axis distances of the scatterer. Moreover, z_n^T and z_n^R are the perpendicular distances from the scatterer to the face of the transmitter and receiver transducers. The product of the magnitude of $H_T(\rho_n^T, \omega, z_n^T)$ and $H_R(\rho_n^R, \omega, z_n^R)$ can be integrated over x , y , and z coordinates to result in the effective cell volume. The subscripts T and R indicate the transmit and receive transducer. Further, $\tau_n = \tau + t_n$ where τ is the travel time for the scatterer at the center of the cell, and t_n is the distance between scatterers n and m .

Considering only the distance between scatterers, Eq. 1 becomes

$$s(t, r) = e^{2\pi j f_o (t-\tau)} \sum_{n=1}^M |H_T(\rho_n^T, \omega, z_n^T)| |H_R(\rho_n^R, \omega, z_n^R)| |\Psi_n(\omega)| |T_T(\omega)| |T_R(\omega)| e^{-2\pi j f_o t_n} \quad (2)$$

and can be further simplified to the random walk formulation

$$s(t, r) = e^{2\pi j f_o (t-\tau)} \sum_{n=1}^M E_n e^{j\phi_n} \quad (3)$$

where $E_n = |H_T(\rho_n^T, \omega, z_n^T)| |H_R(\rho_n^R, \omega, z_n^R)| |\Psi_n(\omega)| |T_T(\omega)| |T_R(\omega)|$ and $e^{\phi_n} = -2\pi j f_o t_n$.

Eq. 3 can be represented as a vector sum of M phasors in the complex plane. Each phasor contributing to the signal has a random amplitude E_n and a random phase, ϕ_n . Each scatterer contributing to the signal must be within the cell volume centered at the cross section of the transmit-receive geometry at 90° as illustrated in Fig. 1.

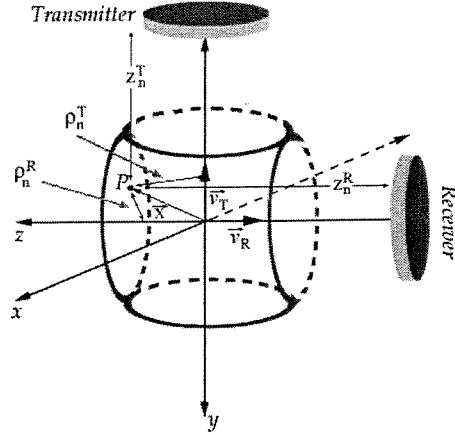


Figure 1: Transmit-receive scanning geometry and the concept of effective cell volume.

The phase at each position n , ϕ_n , is assumed to be statistically independent and uniformly distributed between 0 and 2π . At the same time, the amplitudes at each position n , E_n , are assumed to be statistically independent random variables.⁸

According to Jakeman⁴, the intensity of the signal is equal to the square of the envelope of the field

$$I(t) = |s(t, r)|^2 \quad (4)$$

more importantly, the ratio of the second moment to the square of the first moment of the intensity distribution will be given by

$$\frac{\langle I^2 \rangle}{\langle I \rangle^2} = \frac{2 \langle M(M-1) \rangle}{\langle M \rangle^2} + \frac{\langle E^4 \rangle}{\langle M \rangle \langle E^2 \rangle^2} \quad (5)$$

where $\langle \dots \rangle$ represent the ensemble average and M is the total number of scatterers. Assuming that all scatterers are identical in a given cell volume, and that M obeys a Poisson probability density function where $\langle M(M-1) \rangle = \langle M \rangle^2$, the second normalized intensity moment becomes⁹

$$\frac{\langle I^2 \rangle}{\langle I \rangle^2} = 2 + \frac{\langle E^4 \rangle}{\langle M \rangle \langle E^2 \rangle^2} \quad (6)$$

or, more precisely

$$\frac{\langle I^2 \rangle}{\langle I \rangle^2} = 2 + \frac{\langle |H_T(\rho_n^T, \omega, z_n^T)|^4 |H_R(\rho_n^R, \omega, z_n^R)|^4 \rangle \langle |\Psi_n(\omega)|^4 \rangle \langle |T_T(\omega)|^4 \rangle \langle |T_R(\omega)|^4 \rangle}{\langle M \rangle \langle |H_T(\rho_n^T, \omega, z_n^T)|^2 |H_R(\rho_n^R, \omega, z_n^R)|^2 \rangle^2 \langle |\Psi_n(\omega)|^2 \rangle^2 \langle |T_T(\omega)|^2 \rangle^2 \langle |T_R(\omega)|^2 \rangle^2} \quad (7)$$

where the Lommel diffraction formulation for the transmit-receive transducers, the scattering coefficient and the transmit-receive transfer functions are assumed to be statistically independent.

Assuming ergodicity, where the ensemble average equals its appropriate spatial averages over the cell volume¹⁰, Eq. 7 becomes

$$\begin{aligned} \frac{\langle I^2 \rangle}{\langle I \rangle^2} &= 2 + \frac{\langle |\Psi(\omega)|^4 \rangle \frac{1}{V_T} \langle \langle |H_T(\rho^T, \omega, z^T)|^4 |H_R(\rho^R, \omega, z^R)|^4 \rangle \rangle}{\langle M \rangle \langle |\Psi(\omega)|^2 \rangle^2 \left[\frac{1}{V_T} \langle \langle |H_T(\rho^T, \omega, z^T)|^2 |H_R(\rho^R, \omega, z^R)|^2 \rangle \rangle \right]^2} \\ &= 2 + \frac{\langle |\Psi(\omega)|^4 \rangle}{\langle M \rangle / V_T \langle |\Psi(\omega)|^2 \rangle^2 V_E} \end{aligned} \quad (8)$$

where the $\langle \langle \dots \rangle \rangle$ symbol represents integration over a space that has volume V_T , and V_E is the volume integration. The scatterer number density $\langle M \rangle / V_T$ is a tissue dependent property. At the same time, the term $\frac{\langle |\Psi(\omega)|^4 \rangle}{\langle |\Psi(\omega)|^2 \rangle^2}$ depends on the probability density function of the scattering coefficients at ω , which is also tissue dependent. Together these two terms constitute the “effective scatterer number density” at a frequency ω . Within Eq. 8 there is a term V_E that separates out, and is only dependent on the transducer’s diffraction or beam pattern. We will rewrite V_E as follows:

$$V_E = \frac{\left[\iiint |H_T(x^T, y^T, z^T, \omega)|^2 |H_R(x^R, y^R, z^R, \omega)|^2 dx dy dz \right]^2}{\left[\iiint |H_T(x^T, y^T, z^T, \omega)| |H_R(x^R, y^R, z^R, \omega)| dx dy dz \right]^4} \quad (9)$$

where the transformation from ρ^T, z^T, ρ^R, z^R to x, y , and z coordinate system is explained in section 5.

3. DIFFRACTION EFFECT

To understand the effects of the ultrasound wave on the scattering microstructure we have to examine the pressure field distribution for the focused transducer. O’Neil¹¹ and Kossoff¹² have agreed that the double integration of the Rayleigh expression for the off-axis pressure distribution is complicated, and moreover, as an approximation is satisfactory only when the transducer’s radius is greater than the wavelength. Since then, Penttinen and Luukkala¹³, Madsen et al.¹⁴, Lucas and Muir¹⁵ and Cobb¹⁶ have reduced the solution to a single integral or expressed it as a series. Further, Schmerr et al.¹⁷ have approached this problem by creating a model given in terms of boundary diffraction waves. Another approach for effectively solving the transducer’s pressure field distribution is by implementing a Bessel functions expansion. Recent works by Chen et al.² and Daly¹⁸ have used such expressions in establishing solutions for the pressure field distribution in terms of Lommel functions.

The scatterer number density in Eq. 8 is dependent on the properties of the scattering medium, within a scattering volume, V_E . In order to define this volume it is necessary to consider a monochromatic excitation pulse emerging from a circular aperture and converging towards the axial point O .

According to Fig. 2, the scalar disturbance, $H(\rho, z, \omega)$ at a typical point receiver P , located in the neighborhood of O , where P is generally thought to be at some off-axis distance $\rho = \sqrt{x^2 + y^2}$, can be written as:

$$H(\rho, z, \omega) = \frac{1}{2\pi} \int_{\sigma_o} f(\sigma_o) \frac{e^{-jkr}}{r} d\sigma_o \quad (10)$$

where r is the distance from an element area on the face of the transducer to the point P , and σ_o represents the area of the aperture of the transducer. Furthermore, $f(\sigma_o)$ is the velocity distribution across the face of

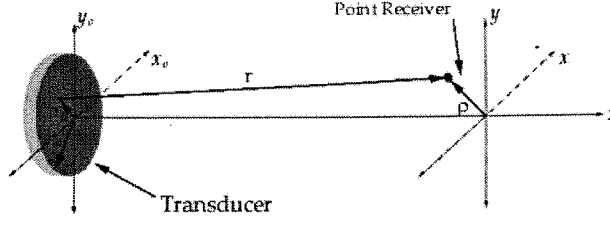


Figure 2: Coordinate system used to calculate the velocity-potential transfer function from a circular aperture.

the transducer. $f(\sigma_o)$ is unity when spatial uniformity is assumed. The subscript o denotes the source plane. The spatial wave number k is defined as the temporal frequency ω over the speed of sound c .

The disturbance $H(\rho, z, \omega)$ is known as the velocity-potential transfer function. The relationship between the impulse response and its transfer function will become apparent when we define the cell volume in section 5.

The circular symmetry of the transducer, and more importantly the Fresnel approximation allows the velocity-potential transfer function in Eq. 10 to be estimated as:

$$\hat{H}(\rho, z, \omega) = \frac{1}{z} e^{-jk(z + \frac{\rho^2}{2z})} \int_0^a e^{-jkr \frac{\rho_o^2}{2z}} J_0\left(\frac{k\rho}{z} \rho_o\right) \rho_o d\rho_o \quad (11)$$

where $\rho_o = \sqrt{x_o^2 + y_o^2}$ is the off-axis distance at the plane of the source. The “hat” notation in $\hat{H}(\rho, z, \omega)$ represents an estimate of the result in Eq. 11. It is convenient to consider separately the real and imaginary parts of the integral in Eq. 11.

$$\int_0^a e^{-jkr \frac{\rho_o^2}{2z}} J_0\left(\frac{k\rho}{z} \rho_o\right) \rho_o d\rho_o = C(u, v) - iS(u, v) \quad (12)$$

where u and v are dimensionless variables that specify the position of point P :

$$u = \frac{ka^2}{z} \quad \text{and} \quad v = \frac{ka\rho}{z}$$

a is the radius of the transducer and z is the distance from the face of the transducer to the axial point O .

According to Born and Wolf¹⁹, the real and imaginary parts of these integrals can be expanded in terms of Bessel functions resulting in the following expressions:

$$\begin{aligned} C(u, v) &= \frac{\sin \frac{1}{2}u}{\frac{1}{2}u} U_1(u, v) + \frac{\cos \frac{1}{2}u}{\frac{1}{2}u} U_2(u, v) \\ S(u, v) &= \frac{\sin \frac{1}{2}u}{\frac{1}{2}u} U_1(u, v) - \frac{\cos \frac{1}{2}u}{\frac{1}{2}u} U_2(u, v) \end{aligned} \quad (13)$$

Further, $U_1(u, v)$ and $U_2(u, v)$ can be calculated in terms of the Lommel functions

$$U_n(u, v) = \sum_{s=0}^{\infty} (-1)^s \left(\frac{u}{v}\right)^{n+2s} J_{n+2s}(v) \quad (14)$$

$$V_n(u, v) = \sum_{s=0}^{\infty} (-1)^s \left(\frac{v}{u}\right)^{n+2s} J_{n+2s}(v) \quad (15)$$

An expression for a focused transducer can be derived similarly by assuming that focussing introduces a time delay in the excitation¹⁸

$$\hat{H}(\rho, z, \omega) = \frac{\epsilon}{kz} e^{-j\left(kz + \frac{k\rho^2}{2z} + \frac{ka^2}{2\epsilon}\right)} [U_1(u, v) + jU_2(u, v)] \quad (16)$$

where $u = ka^2/\epsilon$ and $v = ka\rho/z$, and the time delay is expressed by $1/\epsilon = 1/z - 1/A$ where A is the geometrical focal distance or the radius of curvature of the focused transducer. We will consider a derivation of A and a in the following section. Further, we will refer to \hat{H}_T and \hat{H}_R as the Lommel diffraction formulation for each transmit-receive transducer.

4. THE EFFECTIVE RADIUS AND THE GEOMETRICAL FOCAL LENGTH

As seen in Eq. 16 the Lommel diffraction formulation and in turn the effective cell volume are dependent on two parameters characteristic to the specific transducer used in the experimental part of this work. Therefore, an essential first step is to determine the transducer's effective radius, a , and its effective focal length, or geometrical focal length, A . A number of methods for measuring effective transducer parameters have been tried by Madsen⁸, Amin²⁰, and Lerch¹ among others. We found that Lerch's approach gave a simple yet robust solution to our problem.

The process requires determining the location of the last on-axis null and the on-axis maximum pressure response, which is the location of the transducer's "true focus". By determining both locations we pin down the region of the transducer response where the amplitudes are most significant. In short, Lerch et al.¹ arrived at the following expression for determining the effective radius, a , of the transducer using the null location

$$a = \left[\frac{2z_{\min}\lambda A}{A - z_{\min}} \right]^{1/2} \quad (17)$$

where z_{\min} and A are determined experimentally.

In the above expression the effective radius is not only dependent on the null location z_{\min} , but also on the geometrical focal length A . To calculate A we set the partial derivative with respect to the distance z equal to zero. After lengthy derivation the following expression is reached

$$x \cos x = \frac{\pi - x(z_{\max}/z_{\min})}{\pi - x} \sin x \quad (18)$$

determining the value of root x , allows us to obtain a value for the effective focal length directly by using

$$A = z_{\max} \left[\frac{\pi - x + (\pi^2 - x^2 z_{\min}/z_{\max})/(kz_{\min})}{\pi - x z_{\max}/z_{\min} + (\pi^2 - x^2)/(kz_{\min})} \right] \quad (19)$$

By experimentally determining z_{\min} and z_{\max} at the center frequency of the focused transducer, the intermediate value x can be solved using Eq. 18. Based on this value, the effective focal length or the geometrical focal length can be determined using Eq. 19. The geometrical focal length is then used to calculate the effective radius using Eq. 17.

Table 1 lists an example of the effective parameters derived using the procedure described above based on two sets of experimental values for z_{\min} and z_{\max} for a 2.5MHz focused transducer.

	z_{\min} (cm)	z_{\max} (cm)	Eff. focal length (cm)	Eff. radius (cm)	Center frequency (MHz)
run # 1	2.264	4.728	12.07	0.586	2.5
run # 2	2.311	4.774	11.90	0.594	2.5

Table 1: Effective parameters derived experimentally for a 2.5MHz focused transducer

Fig. 3 shows the experimental on-axis normalized values obtained for the transducer in Table 1, as well as the corresponding on-axis normalized Lommel diffraction formulation values. Although the experimental results in Fig. 3 tend to have an overall agreement with the theoretical calculations, there is an obvious discrepancy between the two. This disagreement is most prominent at the null location where a bias has occurred in the experimental data sets. We speculate that this bias is due to the hydrophone’s finite size used in detecting the transducer’s pulse. Perhaps, another reason for such a bias is the misalignment of the hydrophone with the transducer’s face. Further analysis of this spatially averaging effect can be referred to Daly.¹⁸ Preliminary calculations that included the finite size of the hydrophone as a parameter within the Lommel diffraction formulation showed that the spatial averaging effects do not contribute to any shifts in the null or maxima locations. Moreover, comparison of theoretical calculations and off-axis experiments exhibit significant agreement in both the “true focus” region and geometrical focus region, leading us to believe that the effects of the finite size of the hydrophone does not play a significant role in the effective cell volume calculations. This observation is reflected in Fig. 5, where the effective cell volume in the “true focus” region for the 2.5MHz focused transducer was found to be 195.77mm^3 in the experimental case, while the theoretical calculations yielded 192.35mm^3 . A more detail analysis of these observations will be presented in a future paper.

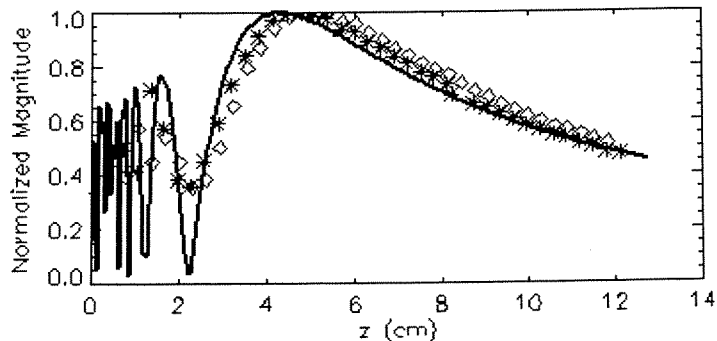


Figure 3. On-axis variation of the velocity-potential for a 2.5MHz focused transducer. Solid line represents the theoretical data, while the symbols represent two experimental data sets.

5. DEFINING THE CELL VOLUME

Once all parameters and appropriate expressions have been defined we can consider the derivation of the effective cell volume, V_E , in Eq. 9. With the previous sections in mind, consider two identical focused transducers placed at 90° from each other. The product of the Lommel diffraction formulation for the transmit-receive geometry yields the point spread function of the scanning system. An illustration of this concept is presented in Fig. 1. In order to calculate the point spread function in each case it is necessary to relate the monochromatic excitation pulse to the point scatterer through a unique coordinate system. Taking the dot product of \vec{x} and unit vector, \vec{v}_T , results in ρ and z values within the x, y, z coordinate system needed to calculate the Lommel diffraction formulation at each point in that system. Similarly, the dot product of \vec{x} and unit vector, \vec{v}_R , results in ρ and z values for the receive case. This process is straight forward, however it can be computationally intensive at times due to the 3D data set in each case. However, because these are identical transducers only one set of calculations is necessary to result in the desired point spread function. In

this case, rigid body rotation of the transmit data set yields the receiver data set within the same coordinate system, eliminating redundant computations.

The theoretical product of the two transfer functions, \hat{H}_T and \hat{H}_R , can be given a physical meaning. Consider a fictitious scattering point, P, located in the vicinity of the crossbeam geometry of the transmit-receive transducers. If the transmitter were to be driven by a unit amplitude sinusoidal signal with frequency ω_o , the received signal amplitude will result in the magnitude of $\hat{H}_T(x_o, y_o, z_o, \omega_o)\hat{H}_R(x_o, y_o, z_o, \omega_o)$, where (x_o, y_o, z_o) are the coordinates of point P. On the other hand, scanning point P, by moving the transmit-receive assembly to various points (x, y, z) in 3D space will result in a signal amplitude $P(x, y, z, \omega_o)$. Therefore, $P(x, y, z, \omega_o)$ becomes the Point Spread Function (PSF) of the scanning system, at frequency ω_o .

$$P(x, y, z, \omega_o) = \left| \hat{H}_T(x, y, z, \omega_o) \right| \left| \hat{H}_R(x, y, z, \omega_o) \right| \quad (20)$$

Eq. 20 is directly related to the effective cell volume, V_E , in the normalized intensity moments expression defined earlier in Eq. 8. To calculate the effective cell volume, we compute $\hat{H}_T(x, y, z, \omega_o)$ at several consecutive x , y , and z values in a desired region, by using the above procedure. The result of this computation is a cube of velocity potential values at each consecutive ρ and z within the coordinate system. Because two identical transducers are used in this example, $\hat{H}_R(x, y, z, \omega_o)$ can be derived from the $\hat{H}_T(x, y, z, \omega_o)$ cube through a 90° rotation about the x axis. To numerically integrate V_E we will write Eq. 9 in discrete form.

$$V_E = \frac{(\Delta x \Delta y \Delta z)^2 \left[\sum_i \sum_j \sum_k |H_T(i, j, k)|^2 |H_R(i, j, k)|^2 \right]^2}{\Delta x \Delta y \Delta z \sum_i \sum_j \sum_k |H_T(i, j, k)|^4 |H_R(i, j, k)|^4} \quad (21)$$

Dimensionally, this expression, does indeed describe a volume:

$$V_E = \frac{(\Delta x \Delta y \Delta z)^2 \left[\sum_i \sum_j \sum_k |H_T(i, j, k)|^2 |H_R(i, j, k)|^2 \right]^2}{\Delta x \Delta y \Delta z \sum_i \sum_j \sum_k |H_T(i, j, k)|^4 |H_R(i, j, k)|^4} = \frac{(m^3)^2}{m^3} \left[\frac{(m^2 m^2)^2}{m^4 m^4} \right] = m^3$$

As a result, the effective cell volume, V_E , can be derived from the actual values of the velocity-potential transfer function at each point in the 3D space. Notice that the transducers' frequency response $T_T(\omega)$ and $T_R(\omega)$ as well as the frequency dependent scattering coefficient $\Psi(\omega)$ have dropped out during the normalization process of the effective cell volume expression, leaving only the system dependent parameters, $H_T(i, j, k)$ and $H_R(i, j, k)$.

Fig. 4 illustrates the 3D PSF in the "true focus" region as well as in the geometrical focus region. Note that in the "true focus" region the PSF resembles a cube with rounded corners, a pseudo-cube, while in the geometrical focus region the PSF has additional information at two ends of the pseudo-cube. This additional information is due to the contribution of the side lobes of both velocity-potential functions. In the "true focus" region the functions for the transmit-receive transducers are much tighter, therefore, the overlapping region in the cross beam geometry is merely a result of the main lobe. Such differences will affect the effective cell volume. In the "true focus" region the effective cell volume at 2.5MHz was found to be 192.65mm³, while in the geometrical focus region equals to 1120.80mm³, a significant increase due to the much wider velocity potential main lobe and contribution of the side lobes.

6. VARIATION OF CELL VOLUME WITH FREQUENCY

Eq. 8 shows that the normalized intensity moments are dependent on the effective scatterer number density $\left(\frac{\langle |\Psi(\omega)|^4 \rangle}{\langle M \rangle / V_T \langle |\Psi(\omega)|^2 \rangle^2} \right)$ as well as on the system dependent variable, the effective cell volume, V_E . Computing the effective cell volume at frequencies within the transducer's bandwidth will shed some light on the nature of the statistical distribution of the scatterers within the cell volume. Moreover, by calculating the effective cell

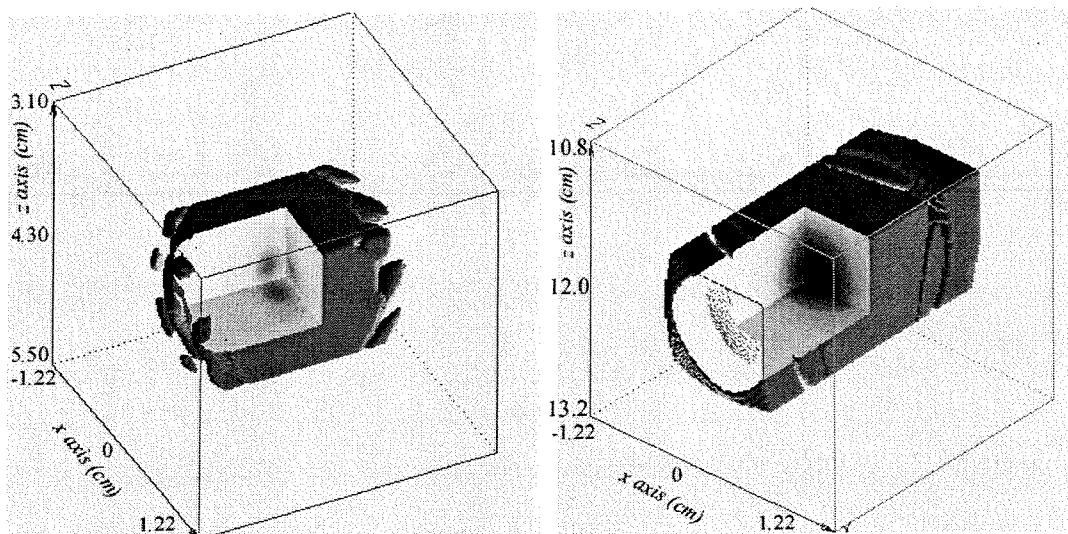


Figure 4. 3D PSF in the “true focus” region (left) and in the geometrical focus region (right) for a 2.5MHz focused transducer.

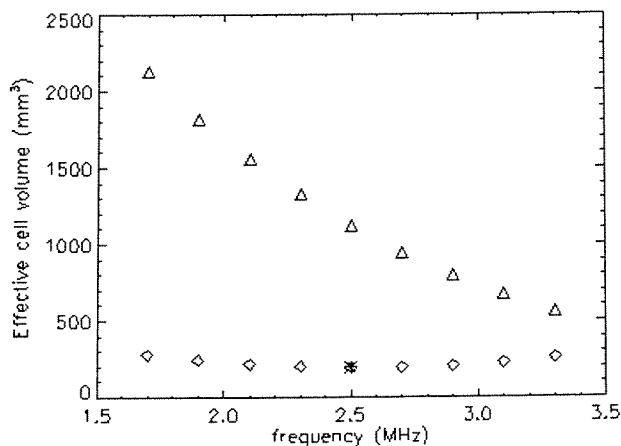


Figure 5. Effective cell volume vs. frequency for the 2.5MHz focused transducer. Diamond symbols represent values in the “true focus” region while the triangle symbols represent values in the geometrical focus region. The asterisk symbol at 2.5MHz represents the experimental result.

volume, V_E , one can investigate the interscatter spacing in the time domain using a method previously derived by Helguera⁸.

Applying the method described in the previous sections we have calculated the effective cell volume, V_E , at 0.2MHz intervals within the experimentally determined transducer’s bandwidth from 1.7MHz to 3.3MHz. The results are illustrated in Fig. 5, where the diamond symbols represent the effective cell volume in the “true focus” location and the triangle symbols represent the effective cell volume in the geometrical focus location. It is clear from Fig. 5 that in the “true focus” location, where the intensity of the beam is most significant, the relationship between frequency and the effective cell volume is fairly constant. However, in the geometrical focus region the effective cell volume decreases significantly as we sweep through frequencies under the transducer’s bandwidth.

7. CONCLUSION

The second normalized intensity moment can be used to convey the statistical nature of scattering structures.

We have shown in Eq. 8 that the second normalized intensity moment depends on the scattering nature of the interrogated structure as well as on the effective cell volume that contains the contributing scatterers. In order to characterize the medium, it is necessary to understand and isolate the contribution of the system dependent variable which we have defined here as the effective cell volume.

In this paper we have considered a crossbeam geometry with separate transmit and receive transducers to compute the effective cell volume V_E in the normalized intensity moments expression. We have developed a relationship between the normalized intensity moments and the effective scatterer number density using monochromatic excitations. Due to the monochromatic nature of the signal we have used the Lommel diffraction formulation to estimate the frequency dependent effective cell volume. Because the Lommel diffraction formulation amounts to a Fresnel approximation to the diffraction integral our approach is valid in the near and far field of the focused circular disk transducers.

The crossbeam geometry used throughout this paper required the transmitter transducer to be at 90° from the receiver transducer. Due to the identical transducer pair and the rigid body rotation of the transmitter data set, the computing time was reduced by half. However, it is important to emphasize that the crossbeam geometry is not limited to the 90° set up, and as a result the effective cell volume V_E , can be computed for any frequency, angle, and depth desired in the experimental world. The experimental validation of alternative crossbeam geometries is the subject of another publication.

8. ACKNOWLEDGEMENTS

The authors would like to thank Dr. D. Dalecki at the University of Rochester department of Biomedical Engineering for the use of the Imotec Messtechnik PVDF Needlehydrophone.

REFERENCES

1. T.P. Lerch, L.W. Schmerr, and A. Sedov, "Characterization of Spherically Focused Transducers Using an Ultrasonic Measurement Model Approach", *Res. Nondestr. Eval.*, **8**, pp. 1-21, 1996.
2. Rao, N.A.N.K., *Encyclopedia of Imaging Science and Technology*, pp. 1412-1435, Ed. J.Hornak, John Wiley & Sons, 2002.
3. X. Chen, K.Q. Schwarz, and K.J. Parker, "Radiation Pattern of a Focused Transducer: A Numerically Convergent Solution", *J. Acoust. Soc. Am.*, **94**, pp. 2979-2991, 1993.
4. E. Jakeman, P. N. Pusy, "A Model for Non-Rayleigh Sea Echo", *IEEE Trans. Antenna & Propagation*, **AP-24**, pp. 806-814, 1976.
5. J.F. Chen, A. Zagzebski, and E. L. Madsen, "Non-Gaussian versus Non-Rayleigh Statistical Properties of Ultrasound Echo Signals", *IEEE Trans. Ultra. Ferro. Freq. Con.*, **41**, pp. 435-440, 1994.
6. R.C. Waag, "A Review of Tissue Characterization from Ultrasonic Scattering", *IEEE Trans. Biomed. Eng.*, **BME-31**, pp. 884-893, 1984.
7. J.A. Campbell, R. C. Waag, "Normalization of Ultrasonic Scattering Measurements to Obtain Average Differential Scattering Cross Sections for Tissues", *J. Acoust. Soc. Am.*, **74**, pp. 393-399, 1983.
8. M. Helguera, *Non-Rayleigh Ultrasonic Characterization of Tissue Scattering Microstructure via a Multi-bandwidth Probing Technique*, Ph.D Dissertation, Chester F. Carlson Center for Imaging Science, Rochester Institute of Technology, 1999.
9. K.A. Wear, R.F. Wagner, and D.G. Brown, "Statistical Properties of Estimates of Signal-to-Noise Ratio and Number of Scatterers per Resolution Cell", *J. Acoust. Soc. Am.*, **102**, pp. 635-641, 1997.
10. A. Papoulis, *Probability, Random Variables, and Stochastic Processes*, p. 246, McGraw-Hill International Edition., 1984.
11. H. T. O'Neil, "Theory of Focusing Radiators", *J. Acoust. Soc. Am.*, **21**, pp. 516-526, 1949.
12. G. Kossoff, "Analysis of Focusing Action of Spherically Curved Transducers", *Ultra. in Med. & Bio.*, **5**, pp.359-365, 1979.

13. A. Penttinen, M. Luukkala, "The Impulse Response and Pressure Nearfield of a Curved Ultrasonic Radiator", J. Phys. D: Appl. Phys., **9**, pp.1547-1557, 1976.
14. E.L. Madsen, M.M. Goodsitt, and J.A. Zagzebski, "Continuous Waves Generated by Focused Radiators", J. Acoust. Soc. Am., **70**, pp.1508-1517, 1981.
15. B.G. Lucas, T.G. Muir, "The Field of a Focusing Source", J. Acoust. Soc. Am., **72**, pp.1289-1296, 1982.
16. W.N. Cobb, "Frequency Domain Method for Prediction of the Ultrasonic Field Patterns of Pulsed, Focused Radiators", J. Acoust. Soc. Am., **75**, pp. 72-79, 1984.
17. L.W. Schmerr, A. Sedov, and T.P. Lerch, "A Boundary Diffraction Wave Model for a Spherically Focused Ultrasonic Transducer", J. Acoust. Soc. Am., **101**, pp. 1269-1277, 1997.
18. C.J. Daly, N.A.H.K. Rao, *Scalar Diffraction from a Circular Aperture*, Kluwer Academic Publishers, 2000.
19. M. Born, E. Wolf, *Principles of Optics*, p. 438, Cambridge University Press. 6th Edition., 1980.
20. F. Amin, T.A. Gray, and F.J. Margetan, *Review of Progress in Quantitative Nondestructive Evaluation*, **1**, (D.O. Thompson and D.E. Chimenti, Eds.) Plenum Press. pp. 233-250, 1991.